Biosensors and Bioelectronics 36 (2012) 192–198

Contents lists available at SciVerse ScienceDirect

Biosensors and Bioelectronics

journal homepage: www.elsevier.com/locate/bios

Ag/Au bi-metallic film based color surface plasmon resonance biosensor with enhanced sensitivity, color contrast and great linearity

Chung-Tien Li [a,1], Kun-Chi Lo [a,1], Hsin-Yun Chang [b], Hsieh-Ting Wu [a], Jennifer H. Ho [c,d,e], Ta-Jen Yen [a,*]

[a] Department of Materials Science and Engineering, National Tsing Hua University, No. 101, Section 2, Kuang-Fu Road, Hsinchu 30013, Taiwan ROC
[b] Micro Systems Technology Center, Industrial Technology Research Institute, 8 Gongyan Rd., Liu-jia Shiang, Tainan 734, Taiwan ROC
[c] Graduate Institute of Clinical Medicine, Taipei Medical University, 250 Wu-Hsing Street, Taipei 110, Taiwan ROC
[d] Center for Stem Cell Research, Taipei Medical University-Wan Fang Medical Center, 111 s. 3, Hsing-Long Rd., Taipei 116, Taiwan ROC
[e] Department of Ophthalmology, Taipei Medical University-Wan Fang Medical Center, 111 s. 3, Hsing-Long Rd., Taipei 116, Taiwan ROC

ARTICLE INFO

Article history:
Received 31 January 2012
Received in revised form
6 April 2012
Accepted 10 April 2012
Available online 21 April 2012

Keywords:
Surface plasmon resonance
Bi-metallic film
Sensitivity
Color contrast
Linear detection range

ABSTRACT

In wavelength surface plasmon resonance (SPR) biosensor, the manipulation of SPR dispersion relation by Ag/Au bi-metallic film was first time implemented. Due to the enhanced resonant wavelength shift and the sharper SPR slope of using Ag/Au bi-metallic film, the illuminated color of reflection shows one order of magnitude greater contrast than conventional SPR biosensors. Such an Ag/Au bi-metallic film based color SPR biosensor (CSPRB) allows the detail bio-interactions, for example 100 nM streptavidin, to be distinguished by directly observing the color change of reflection through naked eyes rather than the analysis of spectrometer. In addition to the enhanced sensitivity and color contrast, this CSPRB also possesses a great linear detection range up to 0.0254 RIU, which leading to the application of point-of-care tests.

1. Introduction

Surface plasmon resonance (SPR), the coherent oscillation of electron charges near dielectric/metallic boundaries, is extremely sensitive to a slight variation of dielectric environments by measuring the shifts of corresponding optical signals such as resonant angles, resonant wavelengths, optical phases, or optical intensities. Hence, SPR is widely applied for the biological and chemical analysis (Raether, 1988). As a biosensor, SPR can directly transduce the biomolecular interactions into the optical signals without labeling processes, which not only simplifies the sampling periods, but also avoids the quenching effect in fluorescent labeling process (Wong et al., 2007, 2008). In addition, SPR owns exceptional advantages beyond current immunoassays, such as real-time analysis, rapid diagnosis, non-invasive detection, small sample volume required, the possibility in quantification and the feasibility in combining with various immunotests (Ananthanawat et al., 2011; Gupta et al., 2011; Fernandez et al., 2010), and further enables a high throughput detecting methodology of SPR imaging (SPRI) by allowing the simultaneous multi-array screening (Rothenhausler and Knoll, 1988; Ladd et al., 2008; Puttharugsa et al., 2011).

Since SPRI carries out an opportunity of monitoring the bio-interactions directly through the image contrast displayed on the screen, it is possible to further extend SPR platform from the central laboratorial analysis into the decentralized clinical diagnosis, in particular point-of-care test (POCT) (Brennan et al., 2009; Nelson et al., 2007; Skottrup et al., 2008; Trevino et al., 2009). However, the commonly used intensity SPRI suffers from the confined linear range for detection, deficient image contrast for quantification, and is vulnerable to light source intensity (O'Brien et al., 2001; Otsuki et al., 2005); meanwhile, the scanning SPRI is restricted by the prolonged image reconstruction process and sophisticated optical designs (Yuk et al., 2006; Notcovich et al., 2000; Beusink et al., 2008). Recently, wavelength SPRI demonstrated a color contrast for imaging, in which this color contrast directly stems from the mixture of non-resonant wavelengths. This color SPRI preserves the wide linear detection range under a simplified optical design, and can be easily perceived by human operators (Shen et al., 2007; Singh and Hillier, 2007). Nevertheless, the current color SPRI is not capable to be served for distinguishing the detailed bio-interactions through direct observation, because of the limitation on the color contrast of reflection and sensitivity. As a consequence, enhancement on the color contrast of reflection and sensitivity should be studied in order to extend the application of SPR into a POCT device.

* Corresponding author. Tel.: +886 3 5742171; fax: +886 3 5722366.
E-mail address: tjyen@mx.nthu.edu.tw (T.-J. Yen).
[1] These authors contributed to this work equally.

0956-5663/$ - see front matter © 2012 Elsevier B.V. All rights reserved.
http://dx.doi.org/10.1016/j.bios.2012.04.016

To serve SPR sensing, Au was widely adopted mainly due to its great chemical stability and biological affinity; however, the sensitivity of using Au is modest as comparing with other metals. Ag, on the other side, owns the superior sensitivity than Au but lower chemical stability and biological affinity (Ong et al., 2006; Choi and Byun, 2010; Chen et al., 2011; Zhai et al., 2007; Yuk et al., 2011). Therefore, by employing the bi-metallic structure with Au as the protecting layer and Ag as the sensing layer, one can enhance the sensitivity and preserve the great chemical stability and biological affinity simultaneously. Unlike the sensitivity enhancement by introducing localized SPR (LSPR) interactions (Lyon et al., 1998; Hutter et al., 2001; Yang et al., 2007) or biomolecular mass enhancement approaches (Scarano et al., 2010; Pyo et al., 2005), the Ag/Au bi-metallic film allows the specimen to be disposable and non-specific to immunotests. Hence, a Ag/Au bi-metallic film was studied on intensity SPR in order to promote the sensing and imaging performances, and has been confirmed to present 1.6–3 folds promotion (Yuk et al., 2011; Chen et al., 2011; Zhai et al., 2007; Xia et al., 2011). Nevertheless, sensitivity enhancement of Ag/Au bi-metallic film on intensity SPR is always accompanied with the decreased linear detection range, and thus limits the bio-interaction species and quantification.

Here we proposed the Ag/Au bi-metallic film based color SPR biosensor (CSPRB), which is the first time demonstration of the enhancements on color contrast and sensitivity, and preserve the great linear detection range simultaneously by Ag/Au bi-metallic film on wavelength SPR. We first numerically discussed the sensitivity enhancement and linearity of four commonly used SPR interrogations (i.e., angle, intensity, phase, and wavelength) when applying Ag/Au bi-metallic film. The simulation results indicate that only wavelength interrogation shows both a sensitivity enhancement and good linearity. Next, we experimentally demonstrated that the Ag/Au bi-metallic film yields 2.54 folds enhancement in resonant wavelength shift, and up to 10 folds enhancement in color contrast of reflection for direct observation in comparison with Au film. With this enhancement, the dynamic biotin–streptavidin binding process with 100 nM streptavidin is discernible for direct observation through the color contrast of reflection. We believe that the Ag/Au bi-metallic film based CSPRB with enhanced color contrast and sensitivity, and the great linear detection range is capable to be applied as POCT devices for decentralized diagnosis.

2. Sensitivity enhancement and linearity of four SPR interrogations by applying Ag/Au bi-metallic film

SPR under Kretschmann–Raether configuration can be conducted by four interrogations, which are angle, intensity, phase, and wavelength interrogations. Here we numerically investigated the sensitivity enhancement and linearity of these four interrogations by applying Ag/Au bi-metallic films. A simulation model based on Fresnel equations was constructed, the resonant (or incident) wavelength was set as 633 nm, and the refractive indices of a prism and an analyte were set as 1.78 and 1.33, respectively. We examined the performance of the Ag/Au bi-metallic film with three total thicknesses of 42, 49 and 56 nm and with 15 different ratios of Ag/Au, in which the dielectric constants of Au and Ag were polynomial fitted according to Johnson's work (Johnson and Christy, 1972). Besides, sensitivity is defined as the ratio of resonant shift to the refractive index change, where the resonant shift depends on the interrogations. Linearity here refers to the linear deviation of resonant shift within 0.01 RIU refractive index changes, which was calculated through the equation proposed by Xia's work (Xia et al., 2011). Linear detection range is larger when this value approaches to zero.

In angle interrogation, the sensitivities decrease as increasing the ratio of Ag/Au in three Ag/Au bi-metallic film thicknesses, as shown in Fig. 1(a). Since SPR excited by a greater wave vector along propagating direction possesses a larger resonant angle shift according to the SPR dispersion relation, under a monochromatic incidence the greater wave vector excitation can be achieved by the metal with larger real part of dielectric constant, and thus Au shows higher sensitivity than Ag (Homola et al., 1999). Besides, the linearity approaches to zero when Ag/Au ratio becomes higher in three Ag/Au bi-metallic film thicknesses, which indicates that the adoption of Ag/Au bi-metallic film will enlarge the linear detection range in angle interrogation. In intensity interrogation, Fig. 1(b) shows that the sensitivities are increased along with the Ag/Au ratio in three Ag/Au bi-metallic film thicknesses. This is because that the sensitivity of intensity interrogation is dominated by the slope of SPR curve, and the slope is greater in Ag than Au (Ehler and Noe, 1995; Choi and Byun, 2010), therefore, the higher ratio of Ag in bi-metallic film will generate the greater slope, and results in the higher sensitivity. Nevertheless, once the slope becomes greater, the linear detection range becomes narrower due to the much severe intensity variation on SPR curve. Hence, the value of linearity becomes larger with the higher Ag/Au ratio. Moreover, if we compared the bi-metallic film thicknesses with 42, 49, and 56 nm in Fig. 1(b), the sensitivity enhancement in 56 nm is greater than 42 and 49 nm. This is because the slope of SPR curve is determined by internal damping and radiation damping, and radiation damping is the function of metallic film thickness, therefore, sensitivity enhancement of different metallic film thickness is not identical. (Li et al., 2009).

Next, in phase interrogation (Fig. 1(c)), the slope of phase transition relies on SPR coupling efficiency mostly (Nelson et al., 1996) and thus, there is no dependency between sensitivity and Ag/Au ratio. The random distribution of linearity vs. Ag/Au ratio suggests that phase interrogation is suitable for trace measurement rather than wide-range detection. In wavelength interrogation, Fig. 1(d) shows that the sensitivities are increased as the Ag/Au ratios become greater in three Ag/Au bi-metallic film thicknesses. Since SPR excited by a smaller wave vector possesses the larger resonant wavelength shift according to the SPR dispersion relation, under a fixed incident angle and continuous incident wavelengths, the smaller wave vector excitation can be achieved by the metal with smaller real part of dielectric constant, hence, Ag shows higher sensitivity than Au (Homola et al., 1999). In addition, Fig. 1(d) shows that the value of linearity becomes larger when the Ag/Au ratio becomes higher, however, the linearity does not exceed 20% during the entire Ag/Au compositions. Different from the intensity and phase interrogations, Ag/Au bimetallic films with 42, 39, and 56 nm show the similar sensitivity enhancement in wavelength interrogation. In summary, Ag/Au bi-metallic film is capable to enhance the sensitivity on intensity, phase, and wavelength interrogations; however, only wavelength interrogation provides best linearity, meanwhile, the sensitivity enhancement is insensitive to the metallic film thickness offset. These characters suggest that sensitivity enhancement of Ag/Au bi-metallic film on wavelength interrogation is suitable for wide-range analysis and mass production.

3. Materials and method

3.1. Chemicals and reagents

10× phosphate buffered saline (PBS, pH: 7.4 ± 0.05) without magnesium and calcium was purchased from Biowest (France).

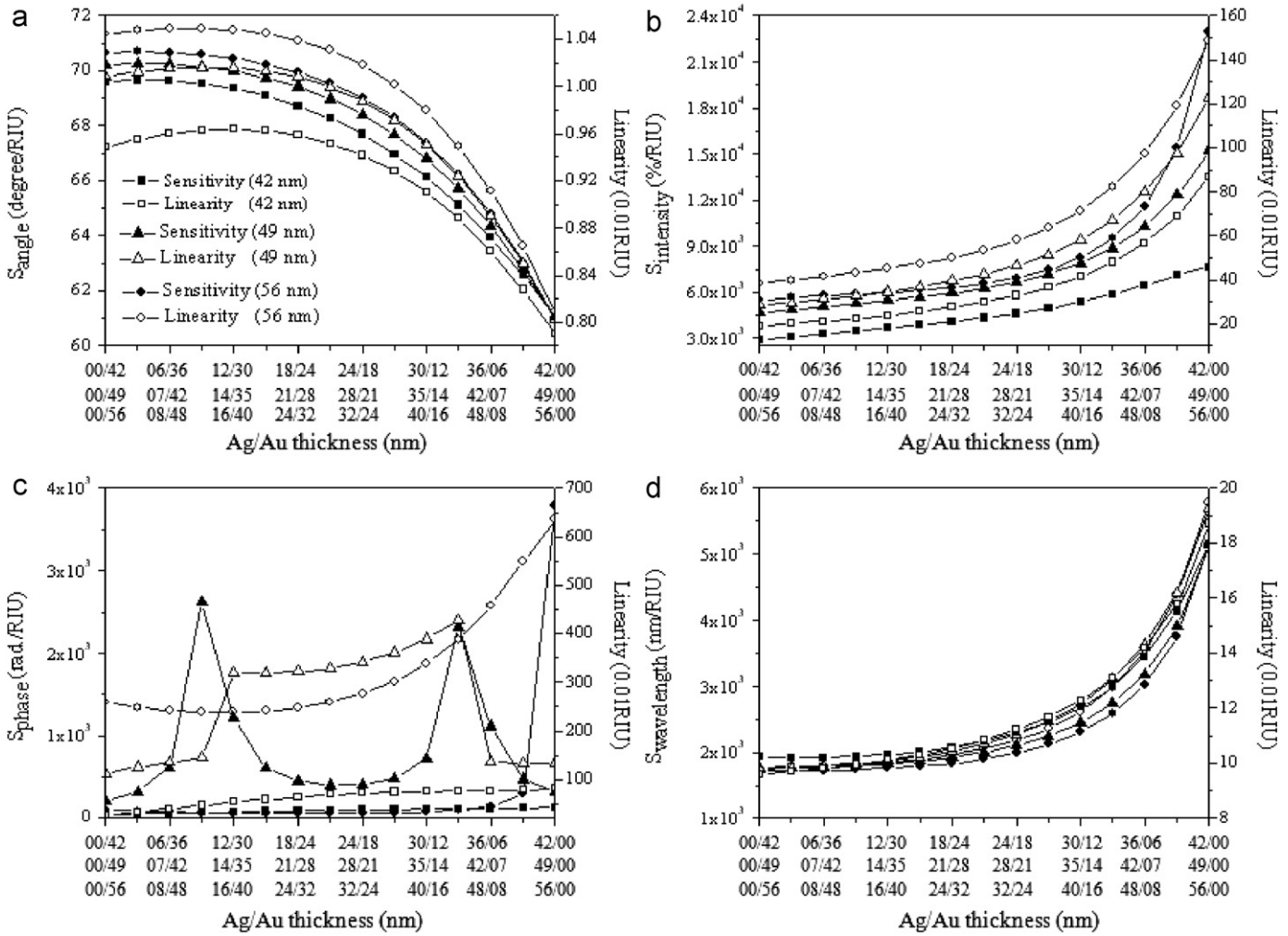

Fig. 1. Sensitivity enhancement and linearity of four SPR interrogations by using Ag/Au bi-metallic film. (a) Angle interrogation; (b) intensity interrogation; (c) phase interrogation; (d) wavelength interrogation.

The dilution of PBS with double distilled water into 1× was mixed before use. Mercaptopropionyl poly(ethylene glycol)-biotin stabilized with disulfide was purchased from LCC Engineering & Trading GmbH (Switzerland). Streptavidin was purchased from Sigma-Aldrich® (*Streptomyces avidinii* as precursor, S4762-5MG, USA). D-(+)-Glucose was obtained from Riedel-deHan® (German). The index matching fluid was purchased from Cargille Labs (refractive index as 1.78, Series M, USA).

3.2. Glucose solution and biotin–streptavidin binding model preparation

For detecting the concentration change of a homogenous solution, glucose with increasing concentrations (0.1, 0.2, 0.3, 0.4, 0.5, 1.0, and 2.0 M) were prepared. The relation between glucose concentration and the corresponding refractive index is originated from Maier's work (Maier et al., 1994). Glucose solutions were injected into the flow chamber at a flow rate of 7.5 μl/min. For the specific binding test, biotin–streptavidin model was demonstrated. Mercaptopropionyl PEG—biotin was first mixed with 4 ml absolute ethanol to yield 1×10^{-3} M biotin solution. Next, glass substrate with metallic film deposition was immersed into as-prepared biotin solution for 24 h at 25 °C. A self-assembling biotinylated monolayer was formed on the metallic film. Streptavidin stock solution with 1×10^{-5} M concentration was first prepared by mixing with 1.5 ml PBS solution, and was carefully stored at −20 °C before use. For the dynamic binding process of biotin–streptavidin model, 100 nM streptavidin solution was prepared by the mixture of 10 μl streptavidin stock solution and 1000 μl PBS, and was injected into the flow chamber at a flow rate of 7.5 μl/min.

3.3. Preparation of metallic film

SF-11 glass substrates (refractive index: 1.78) were first cleaned by using four cleaning agents including commercial detergent water solution, 95% ethanol, acetone, and isopropanol. Between each treatment of cleaning solution, the glass substrates were rinsed and sonicated in DI water. Metallic films were deposited on SF-11 glass substrates by electron beam evaporator with the deposition rate as 0.5 Å/s and the pressure lower than 3.5×10^{-6} mbar. In the Ag/Au bimetallic film, Ag with optimized thickness was first deposited, and followed by a thin Au film. Both Ag/Au bi-metallic film and Au film were first deposited by 3 nm Ti for better adhesion. The as-deposited substrates were reserved in ethanol prior to use. Metallic film thicknesses were monitored by quartz crystal microbalance (QCM) during the deposition, and measured by atomic force microscopy (AFM) after the deposition procedure.

3.4. Optical configuration of Ag/Au bi-metallic film based color SPR biosensor

The optical configuration of Ag/Au bi-metallic film based CSPRB is shown in Fig. 2. Continuous light emitted by a white light emitting diode (LED) was first collimated by the convex lens pair and aperture. The incident light passed through the linear polarizer for TE/TM polarization mode selection. The 400 μm pin-hole was used to minimize the incident beam size before the incident light impinged on the SF-11 cylindrical prism under attenuated total internal reflection (ATR) configuration. The reflection was recorded by the CCD camera (DS-5Mc, Nikon Inc.) after passing through the convex lens. Besides, the reflection spectra were collected alternatively by the spectrometer (HR-4000, Ocean Optics Inc.) in order to investigate the resonant wavelength. In the reflection spectra of TE and TM polarized waves, the TE spectrum refers to the original LED spectrum and the TM spectrum is deformed by the excitation of SPR (Supplementary Fig. S1). From the intensity ratio between TE and TM spectra, SPR curves were generated and the resonant wavelengths can be modified by sweeping the incident angles. In this work, the Ag/Au bi-metallic film with optimized thickness and the commonly used 50-nm Au film were examined.

The illuminated colors of TM polarized reflections recorded by the CCD camera shows distinct colors when the resonant wavelength was adjusted by tuning incident angles (Supplementary Fig. S2). The color of reflection was composed by the sum of non-resonant wavelengths; hence, the illuminated color of reflection will be changed once the resonant wavelength is shifted by the introduced analytes. When the resonant wavelength is 624 nm, the reflection is majorly composed by the wavelengths ranged from 500 to 600 nm, and thus resulted in the green color (Supplementary Fig. S2). As the resonant wavelength was tuned to 555 nm by increasing the incident angle, the reflection was composed by the three separated peaks, in which the peak maximum located at 447.74, 520.46, and 615.83 nm (Supplementary Fig. S1), and resulted in the red color. In order to enhance the color contrast for eyepieces discrimination, we set the resonant wavelength at 555 nm due to two reasons. First, the maximum intensity of our LED spectrum was located at 568.15 nm, which means the wavelength shift vicinity to this wavelength will generate significant intensity variation than other wavelengths, and contribute to the color contrast of reflection. Second, the eye sensitivity function in the photopic vision regime is reported maximized at 555 nm (International Commission on Illumination, CIE 1931), and thus the color variation nearby 555 nm will be much distinguishable for naked eyes.

3.5. Optimization of Ag/Au bi-metallic film

We used 5-nm Au film as the protection layer of Ag/Au bi-metallic film, because the roughness of Ag film after deposition

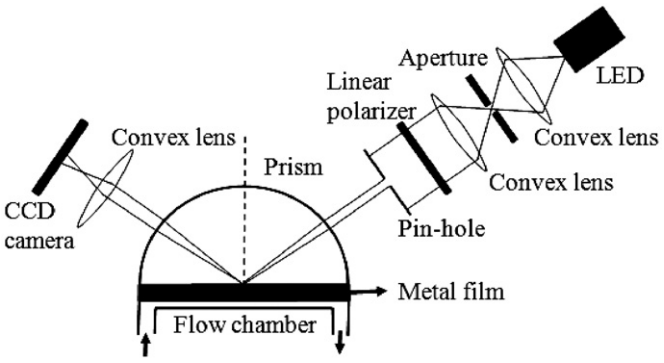

Fig. 2. Optical configuration of color SPR system.

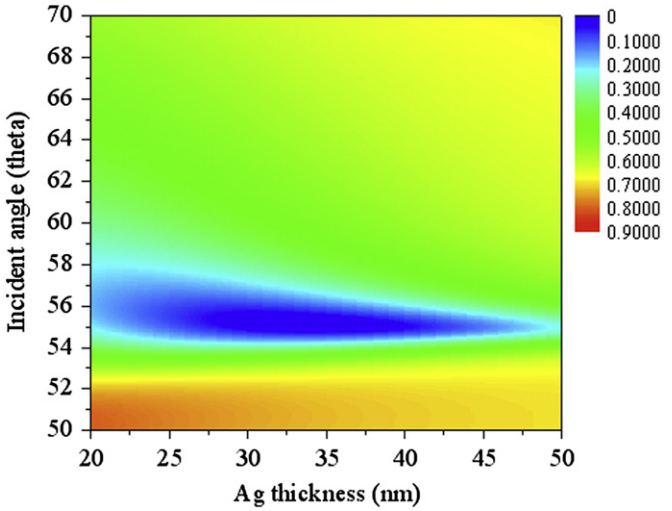

Fig. 3. The SPR reflection vs. Ag thicknesses and incident angles. The color represents the reflectivity at 555-nm wavelength. (For interpretation of the references to color in this figure legend, the reader is referred to the web version of this article.)

was measured as 1.484 nm, therefore, 5-nm Au film was considered thick enough to bury Ag layer. In addition, the chemical stability test also shows that 5-nm Au film is sufficient to provide chemical resistance (Supplementary Fig. S3). Under the circumstances of 5-nm Au film as protection layer and 555-nm resonant wavelength as ideal chromatic condition, we simulated the optimized Ag film thickness and incident angle. As shown in Fig. 3, Ag film with 35 nm thickness under 55° incidence shows the best coupling efficiency (i.e., minimum reflectivity in the color distribution), accordingly, Ag/Au bi-metallic film with 35-nm Ag and 5-nm Au and under 55° incidence was served for Ag/Au bi-metallic film based CSPRB. For the 50-nm Au film, the incident angle was set as 62° to obtain 555-nm resonant wavelength. We then compared the SPR curves of 35/5-nm Ag/Au bi-metallic film and 50-nm Au film (Supplementary Fig. S4). The SPR curve of Ag/Au bi-metallic film shows the larger resonant wavelength shift than Au film, and the sensitivity is calculated as 1949.5 nm/RIU, which are 3.58 folds higher than Au film. The adoption of Ag/Au bi-metallic film is not only beneficial to the resonant wavelength shift but also the slope of SPR curve. The greater slopes generated by Ag/Au bi-metallic film provided a much acute intensity variation than Au film, and will reinforce the intensity variation nearby the resonance.

4. Results and discussions

4.1. Sensitivity and linearity of Ag/Au bi-metallic film based CSPRB

Here we introduced glucose solution with increasing concentrations to study the sensitivity and the linearity of Ag/Au bi-metallic film based CSPRB. Fig. 4 shows the resonant wavelength shifts of the Ag/Au bi-metallic film and the Au film along with refractive index changes, where the resonant wavelength in both cases were modulated at 555 nm in water before tests. In Fig. 4, the Ag/Au bi-metallic film with 35/5 nm thicknesses exhibited 2.53 folds higher sensitivity than the common used 50-nm Au film. The modest sensitivity of Ag/Au bi-metallic film in experiments (i.e., 1266.3 nm/RIU in Fig. 4) in comparison with the simulation result (i.e., 1949.5 nm/RIU in Fig. 3(b)) is considered due to the offset of Ag/Au thickness ratio during the deposition process, because the sensitivity of bi-metallic film is substantially

changed as the Ag/Au thickness ratio approaching to infinite (i.e., pure Ag) in accordance with Fig. 1(d). Besides, the linearity of Ag/Au bi-metallic film and Au film in Fig. 4 are 13.94% and 23.75% respectively, and the linear range is up to 0.0254 RIU in both cases. This fact confirms that the sensitivity enhancement of bi-metallic film did not shorten the linear detection range in wavelength interrogation. Furthermore, we injected water and 0.3 M glucose solution alternatively to test the reusability, and the results show that the glucose was not accumulated on the metal surface during the experiments (Supplementary Fig. S5). In summary, Ag/Au bi-metallic film based CSPRB preserves the great linear detection range, and allows SPR to be served for variety biosensing matrices and immunospecies with different order of refractive indices change, and also permits the quantification.

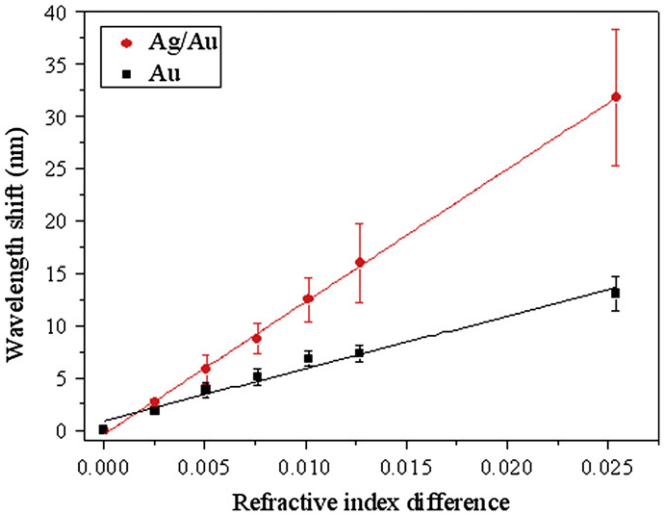

Fig. 4. Sensitivity and linearity of Ag/Au bi-metallic film based CSPRB. Different concentrations of glucose were injected to generate the refractive index changes.

4.2. Ag/Au bi-metallic film based CSPRB in monitoring glucose concentrations

The increasing refractive index changes caused by glucose solutions led to the absorption shift and the intensity variation of the TM polarized reflections (Fig. 5(a)). In the case of Ag/Au bi-metallic film, wavelength peaks at 523.8 and 624.8 nm shifted to longer wavelengths along with the increasing glucose concentrations, and the intensity of the peak at 523.8 nm was increased, whereas the intensity of the peak at 624.8 nm was decreased. The resonant wavelength shifts and the acute intensities variation of these two peaks reflected on the illuminated color of reflections (Fig. 5(b)). From the illuminated colors, the color of DI water was dominated by the peak at 624.8 nm, and thus showed the red color. As the glucose concentration increased to 1.0 M, the wavelength peaks at 523.8 nm dominated the illumination, and thus displayed the green color. In addition, the yellow color in 2.0 M represents that the resonant wavelength was shifted to 642.9 nm, and the illumination was dominated by the wavelength peak at 560.7 nm. The minimum resolving color contrast in Fig. 5(b) is from 0 to 0.2 M glucose concentrations, which corresponds to 5.08×10^{-3} RIU. In the case of Au film, wavelength peak shifts and intensities variation at 523.9 and 616.7 nm showed the similar behaviors to Ag/Au bi-metallic film, however, the shift of resonant wavelength and the change of intensity are smaller than Ag/Au bi-metallic film. From the illuminated colors (Fig. 5(c)), the critical resolving concentration in Au film is 2.0 M, which corresponds to 5.08×10^{-2} RIU. As a consequence, in terms of the color contrast the critical resolution of Ag/Au bi-metallic film is 10 folds greater than Au film, and is 3.96 folds greater than the sensitivity enhancement of resonant wavelength shift as

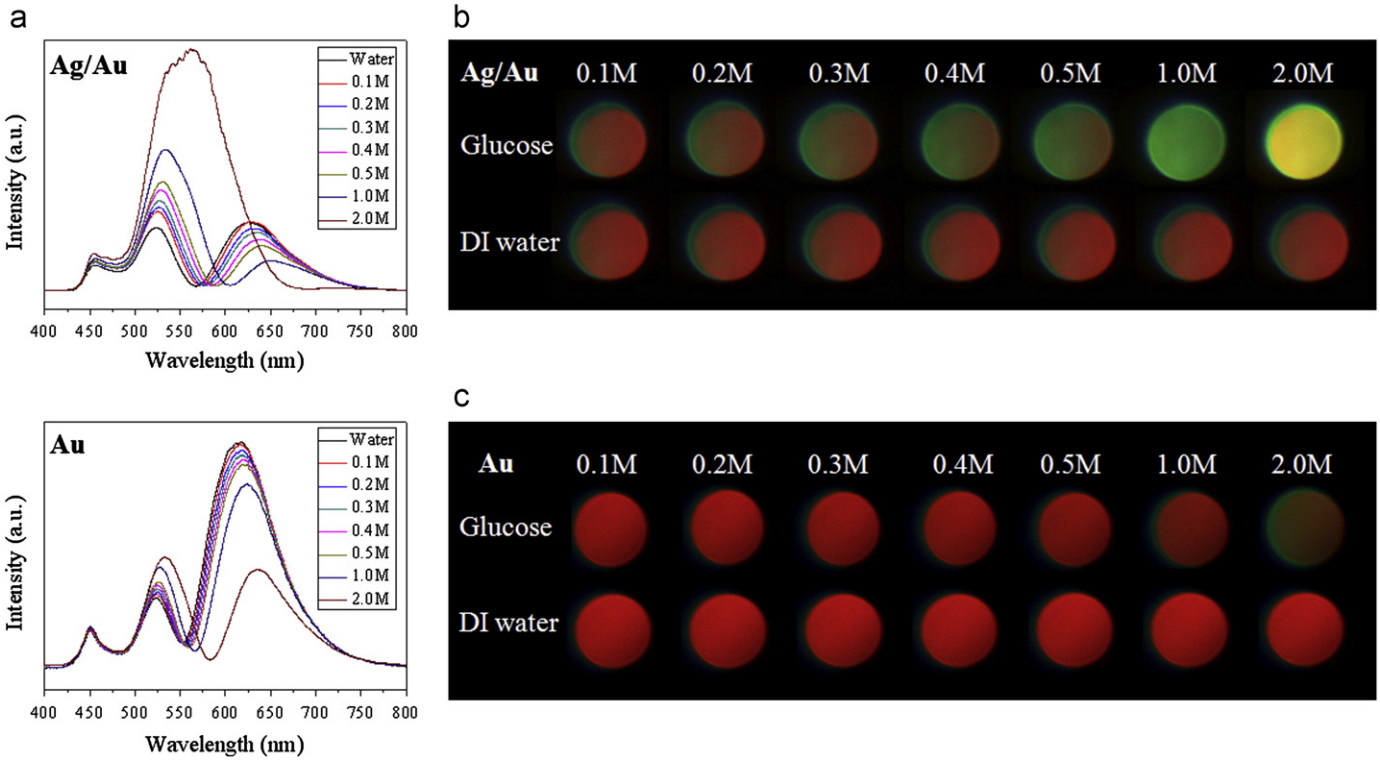

Fig. 5. Ag/Au bi-metallic film based CSPRB in monitoring glucose concentrations. (a) TM spectra of the reflection of Ag/Au bi-metallic film and Au film; (b) illuminated colors of reflections of different glucose concentrations in Ag/Au bi-metallic film case; (c) illuminated colors of reflections of different glucose concentrations in Au film case. (For interpretation of the references to color in this figure legend, the reader is referred to the web version of this article.)

shown in Fig. 4. This additional enhancement in color contrast is attributed to the narrower bandwidth of SPR curve in Ag/Au bi-metallic than Au film. Since the slope of SPR curve affects the intensity variation vicinity to the resonant wavelength, the SPR curve with greater slope will generate the larger intensity variation of non-resonant wavelengths in reflection, and eventually improve the color contrast.

4.3. Ag/Au bi-metallic film based CSPRB in monitoring biotin–streptavidin binding model

Here we monitored the dynamic binding process of biotin–streptavidin model by Ag/Au bi-metallic film based CSPRB. In Fig. 6(a), 100 nM streptavidin solution was introduced into flow chamber with the flow rate as 7.5 μl/min. The biotin–streptavidin interaction generated a 12 nm wavelength shift in Ag/Au bi-metallic film and a 5 nm wavelength shift in Au film. The wavelength shift in Ag/Au bi-metallic film is 2.4 folds greater than Au film, which matches with the sensitivity enhancement shown in Fig. 4. In addition, considering the refractive index of streptavidin as 1.45 and the corresponding resonant wavelength shift, the monolayer thickness of streptavidin was calculated as 6.40 nm according to the equation proposed by Jung's works (Jung et al., 1998), which agrees with the measurement results in the literature (Busse et al., 2002). The dynamic process of biotin–streptavidin interaction was recorded by CCD camera and the illuminated colors were shown in Fig. 6(b). In the serial of Ag/Au bi-metallic film, the reflections before 30 min illuminated red colors, and gradually changed from red to green color during 40–60 min. The distinct color contrast of reflections before and after bio-interactions indicates that streptavidin formed the binding with biotin that attached on the substrate. On the other side, the illuminated colors in Au film stayed invariant during the whole interaction due to the insufficient color contrast. Consider the minimum resolution of the Ag/Au bi-metallic film based CSPRB as 5.08×10^{-3} RIU for direct observation, the minimum discernible streptavidin concentration is 49.7 nM within the same detecting period. It is worth to mention that the sensitivity enhancement of Ag/Au bi-metallic film directly modulated the SPR dispersion curve through the dielectric constant of metal, which means it is possible to further enhance the sensitivity by introducing a bio-molecule amplification process for DNA hybridization or other trace measurements (Lee et al., 2005; Sato et al., 2006).

5. Conclusions

In this work, we demonstrated the first-ever Ag/Au bi-metallic film based color SPR biosensor (CSPRB) with the enhanced sensitivity and color contrast, and great linear detection range. We first numerically verified the sensitivity and linearity of Ag/Au bi-metallic film with respect to four SPR interrogations (i.e. angle, intensity, phase, and wavelength), manifesting that only wavelength interrogation shows the sensitivity enhancement without decreasing the linear detection range. By employing the optimized Ag/Au bi-metallic film as 35/5 nm thickness, our experimental results confirmed that the shift of resonant wavelengths is enhanced to be 2.54 folds and meanwhile the color contrast becomes 10 folds higher than the commonly used Au film. The extraordinary enhancement in color contrast than sensitivity is attributed to the greater resonant wavelength shift, and the steeper SPR slope of Ag/Au bi-metallic film, so that bio-interactions can be detected by directly monitoring the color change of reflections, even for direct observation. In biotin–streptavidin

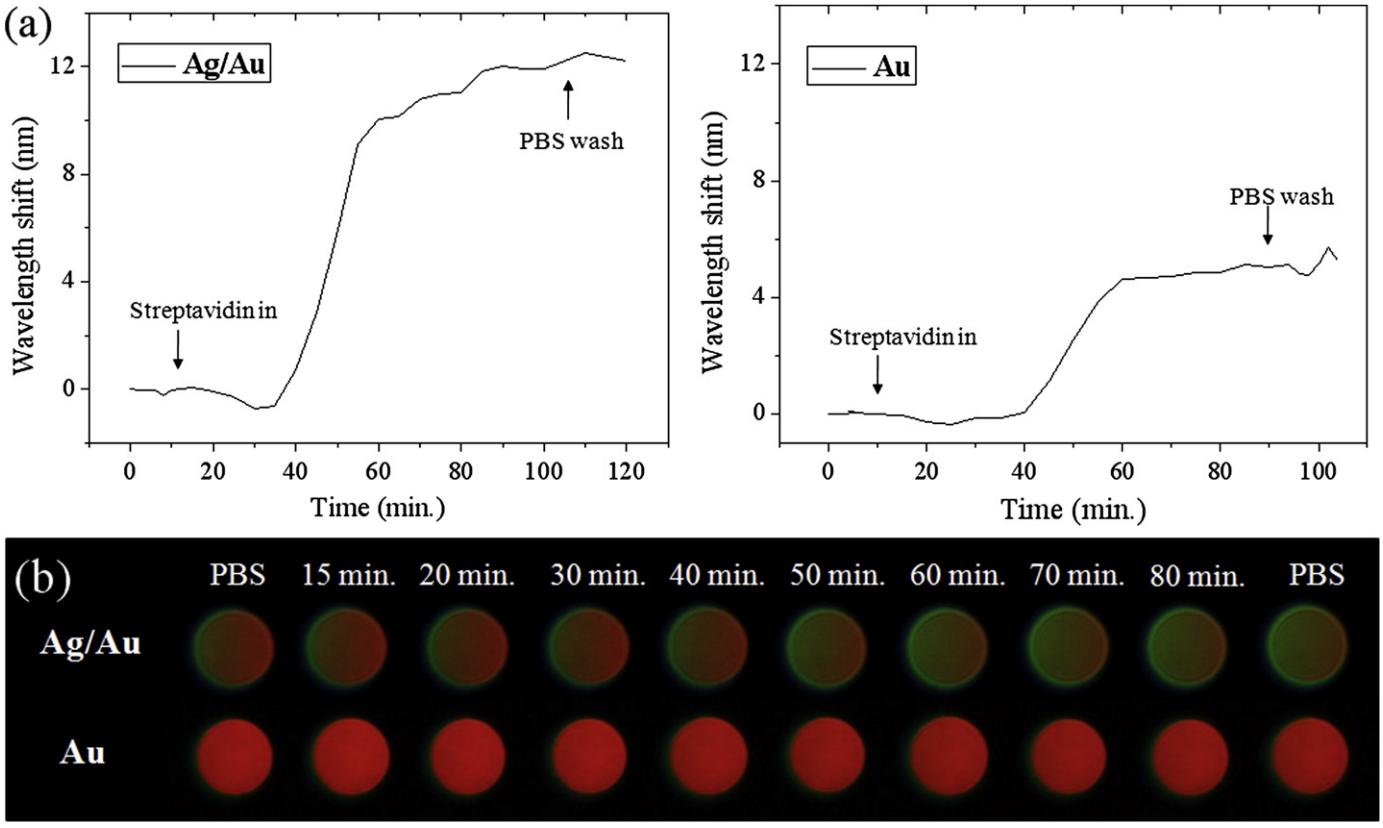

Fig. 6. Ag/Au bi-metallic film based CSPRB in monitoring biotin–streptavidin binding model. (a) Dynamic curves of biotin–streptavidin interaction by using Ag/Au bi-metallic film and Au film; (b) chromatic illuminations of the dynamic interaction by using Ag/Au bi-metallic film and Au film. (For interpretation of the references to color in this figure, the reader is referred to the web version of this article.)

interaction, this enhanced color contrast allows the streptavidin concentration as low as 100 nM being discernible by direct observation, leading this Ag/Au bi-metallic film based CSPRB to the applications of point-of-care tests and others.

Acknowledgments

The authors would like to gratefully acknowledge the financial support from the National Science Council (NSC98-2112-M-007-002-MY3, NSC100-2120-M-002-008, and NSC100-2120-M-010-001), and from the Ministry of Education ("Aim for the Top University Plan" for National Tsing Hua University).

Appendix A. Supporting information

Supplementary data associated with this article can be found in the online version at http://dx.doi:10.1016/j.bios.2012.04.016.

References

Ananthanawat, C., Hoven, V.P., Vilaivan, T., Su, X.D., 2011. Biosensors and Bioelectronics 26 (5), 1918–1923.
Beusink, J.B., Lokate, A.M.C., Besselink, G.A.J., Pruijn, G.J.M., Schasfoort, R.B.M., 2008. Biosensors and Bioelectronics 23 (6), 839–844.
Brennan, D., Justice, J., Corbett, B., McCarthy, T., Galvin, P., 2009. Analytical and Bioanalytical Chemistry 395 (3), 621–636.
Busse, S., Scheumann, V., Menges, B., Mittler, S., 2002. Biosensors and Bioelectronics 17 (8), 704–710.
Chen, Y., Zheng, R.S., Zhang, D.G., Lu, Y.H., Wang, P., Ming, H., Luo, Z.F., Kan, Q., 2011. Applied Optics 50 (3), 387–391.
Choi, S.H., Byun, K.M., 2010. Journal of the Optical Society of America A: Optics, Image Science and Vision 27 (10), 2229–2236.
Ehler, T.T., Noe, L.J., 1995. Langmuir: The ACS Journal of Surfaces and Colloids 11 (10), 4177–4179.
Fernandez, F., Hegnerova, K., Piliarik, M., Sanchez-Baeza, F., Homola, J., Marco, M.P., 2010. Biosensors and Bioelectronics 26 (4), 1231–1238.
Gupta, G., Bhaskar, A.S.B., Tripathi, B.K., Pandey, P., Boopathi, M., Rao, P.V.L., Singh, B., Vijayaraghavan, R., 2011. Biosensors and Bioelectronics 26 (5), 2534–2540.
Homola, J., Koudela, I., Yee, S.S., 1999. Sensors and Actuators B: Chemistry 54 (1–2), 16–24.
Hutter, E., Cha, S., Liu, J.F., Park, J., Yi, J., Fendler, J.H., Roy, D., 2001. The Journal of Physical Chemistry B 105 (1), 8–12.
Jung, L.S., Campbell, C.T., Chinowsky, T.M., Mar, M.N., Yee, S.S., 1998. Langmuir: The ACS Journal of Surfaces and Colloids 14 (19), 5636–5648.
Johnson, P.B., Christy, R.W., 1972. Physical Review B 6 (12), 4370–4379.
Ladd, J., Taylor, A.D., Piliarik, M., Homola, J., Jiang, S., 2008. Analytical Chemistry 80 (11), 4231–4236.
Lee, H.J., Li, Y., Wark, A.W., Corn, R.M., 2005. Analytical Chemistry 77 (16), 5096–5100.
Li, C.T., Yen, T.J., Chen, H.F., 2009. Optics Express 17 (23), 20771–20776.
Lyon, L.A., Musick, M.D., Natan, M.J., 1998. Analytical Chemistry 70 (24), 5177–5183.
Maier, J.S., Walker, S.A., Fantini, S., Franceschini, M.A., Gratton, E., 1994. Optics Letters 19 (24), 2062–2064.
Nelson, K.E., Foley, J.O., Yager, P., 2007. Analytical Chemistry 79 (10), 3542–3548.
Nelson, S.G., Johnston, K.S., Yee, S.S., 1996. Sensors and Actuators B: Chemistry 35 (1–3), 187–191.
Notcovich, A.G., Zhuk, V., Lipson, S.G., 2000. Applied Physics Letters 76 (13), 1665–1667.
Ong, B.H., Yuan, X.C., Tjin, S.C., Zhang, J.W., Ng, H.M., 2006. Sensors and Actuators B: Chemistry 114 (2), 1028–1034.
Otsuki, S., Tamada, K., Wakida, S., 2005. Applied Optics 44 (17), 3468–3472.
O'Brien, M.J., Perez-Luna, V.H., Brueck, S.R.J., Lopez, G.P., 2001. Biosensors and Bioelectronics 16 (1–2), 97–108.
Puttharugsa, C., Wangkam, T., Huangkamhang, N., Gajanandana, O., Himananto, O., Sutapun, B., Amarit, R., Somboonkaew, A., Srikhirin, T., 2011. Biosensors and Bioelectronics 26 (5), 2341–2346.
Pyo, H.B., Shin, Y.B., Kim, M.G., Yoon, H.C., 2005. Langmuir: The ACS Journal of Surfaces and Colloids 21 (1), 166–171.
Raether, H., 1988. Springer-Verlag.
Rothenhausler, B., Knoll, W., 1988. Nature 332 (6165), 615–617.
Sato, Y., Sato, K., Hosokawa, K., Maeda, M., 2006. Analytical Biochemistry 355 (1), 125–131.
Scarano, S., Mascini, M., Turner, A.P.F., Minunni, M., 2010. Biosensors and Bioelectronics 25 (5), 957–966.
Skottrup, P.D., Nicolaisen, M., Justesen, A.F., 2008. Biosensors and Bioelectronics 24 (3), 339–348.
Shen, G.Y., Han, Z.Q., Liu, W., Chen, Y., 2007. Chemistry Letters 36 (7), 926–927.
Singh, B.K., Hillier, A.C., 2007. Analytical Chemistry 79 (14), 5124–5132.
Trevino, J., Calle, A., Rodriguez-Frade, J.M., Mellado, M., Lechuga, L.M., 2009. Analytica Chimica Acta 647 (2), 202–209.
Wong, C.L., Ho, H.P., Suen, Y.K., Kong, S.K., Chen, Q.L., Yuan, W., Wu, S.Y., 2008. Biosensors and Bioelectronics 24 (4), 606–612.
Wong, C.L., Ho, H.P., Yu, T.T., Suen, Y.K., Chow, W.W.Y., Wu, S.Y., Law, W.C., Yuan, W., Li, W.J., Kong, S.K., Lin, C., 2007. Applied Optics 46 (12), 2325–2332.
Xia, L.P., Yin, S.Y., Gao, H.T., Deng, Q.L., Du, C.L., 2011. Plasmonics 6 (2), 245–250.
Yang, X.H., Wang, Q., Wang, K.M., Tan, W.H., Li, H.M., 2007. Biosensors and Bioelectronics 22 (6), 1106–1110.
Yuk, J.S., MacCraith, B.D., McDonagh, C., 2011. Biosensors and Bioelectronics 26 (7), 3213–3218.
Yuk, J.S., Kim, H.S., Jung, J.W., Jung, S.H., Lee, S.J., Kim, W.J., Han, J.A., Kim, Y.M., Ha, K.S., 2006. Biosensors and Bioelectronics 21 (8), 1521–1528.
Zhai, P.M., Guo, J., Xiang, J., Zhou, F.M., 2007. Journal of Physical Chemistry C 111 (2), 981–986.